Send Orders of Reprints at reprints@benthamscience.net

318 *Current Nanoscience,* **2013**, *9*, 318-323

Adsorption Properties of Nanocrystalline/Nanoporous Gallium Nitride Powders

Mariusz Drygas, Jerzy F. Janik and Leszek Czepirski*

AGH University of Science and Technology, Faculty of Energy and Fuels, al. Mickiewicza 30, 30-059 Krakow, Poland

Abstract: A diverse pool of six semiconductor GaN nanopowders was synthesized by the thermally-driven pyrolysis of gallium imide at various temperatures. The XRD-derived average crystallite sizes for the nanopowders were in the range 1-17 nm. Standard nitrogen adsorption measurements at 77 K yielded the basic characteristics of the powder pore structures including the BET surface areas that spanned 23-287 m^2/g. Rare studies of adsorption of water vapor, carbon dioxide, and hydrogen on the nitride nanopowders were carried out. The data on water vapor adsorption at 295 K supported chemisorption of water molecules on the primary adsorption centers and physisorption on the secondary centers. The data on carbon dioxide adsorption at 273 K and hydrogen adsorption at 77 K were used to determine the selectivity of adsorption for these gases defined as the ratio of the respective Henry's constants calculated from the Langmuir equation. The GaN nanopowders showed remarkably diverse pore structure characteristics and adsorption properties that could be linked to the nitride's average crystallite size and crystallite agglomeration, the latter supported by helium density data.

Keywords: Nanocrystalline, GaN, adsorption, water vapor, hydrogen, carbon dioxide.

1. INTRODUCTION

The broad band-gap semiconductors including gallium nitride GaN and its alloys with other Group III(13) nitrides have been widely investigated for their new applications in short wavelength optoelectronics as well as in high-power, high-frequency, and high-temperature electronic devices. These applications dwell on the excellent thermal, mechanical, and chemical stabilities as well as unique electronic properties of GaN such as the broad band-gap (3.4 eV), strong piezoelectric effects (2-6 MV/cm), high saturation velocity ($2.7 \cdot 10^4$ cm/s), and high breakdown field ($2 \cdot 10^6$ V/cm) [1]. In particular, the availability of semiconductor "blue" emmiters based on GaN has given a strong impact for developing applications such as displays, traffic signals, DVD, and data storage [2-3] as well as the next generation of prospect devices including quantum dot lasers, vertical cavity surface emitting lasers, UV light emitting lasers, field effect transistors/bipolar transistors, and spintronic materials [1, 4-7]. Most of these applications utilize single crystals and/or thin films of GaN but in some specific cases, *e.g.*, in chemical and biochemical sensors, porous powder materials are desirable that exhibit a range of properties related to the shift of band-gap, luminescence intensity enhancement as well as photoresponse improvement [8-11]. Porosity and related surface properties of GaN nanopowders appear to play an important role in powder densification *via* compacting/sintering processing [12]. Porous GaN is also a good growth template for epitaxial re-growth which could significantly reduce the density of structural defects allowing for the growth of residual stress-free epitaxial GaN layers [13].

Classic semiconductors (Si, Ge, *etc.*) as porous material forms have been investigated in recent years but there are only scarce publications detailing porosity characteristics/properties of GaN nanopowders [14,15] while many related surface properties of fundamental nature have yet to be refined in the system. In this regard, our earlier study for a limited number of prepared GaN, AlN, and AlGaN powders confirmed them as mostly mesoporous nanocrystalline materials with the BET specific surface areas in the range of up to 300 m^2/g [14]. Also, it provided a strong evidence for chemisorption of water vapor and indicated highly specific adsorption of such gases as carbon dioxide, methane, nitrogen, and oxygen on these nanopowders. To the best of our knowledge, that adsorption study has remained to-date the only published attempt of this kind. Although limited in the number of samples and short of their full characterization, it revealed the nanopowders diverse adsorption behavior towards a variety of gases. One other relevant study known to us has utilized only nitrogen adsorption on GaN-based powders prepared by a comparable route yielding a broad range of preceramic nitride bodies of porosities ranging from prevailing microporosity to mesoporous characteristics and specific surface areas in the similar range as mentioned above [15]. Clearly, a systematic study of adsorption properties for a well-defined range of GaN nanopowders and suitable adsorption gases is needed to clarify a nature of the nitride pore structure and its response to various gases. In this regard, our to-date experience based on the investigation of a wide range of GaN nanopowders supports a model of porosity for such systems in terms of surfaces and interparticle volumes of closed-packed equidimensional crystallites and/or their agglomerates, and a detailed account of such a model has just been published [16].

The main goal of this study was a multipronged characterization of the pore structure and adsorption properties of GaN powders spanning a wide range of average crystallite sizes in the low nanosized region. This kind of structural information and the knowledge on the nature of porosity in GaN nanopowders were not available at the time of our initial publication nor were done comprehensive adsorption studies for various gases [14]. In this report, the information about the specific surface area and pore volumes was derived from standard nitrogen adsorption determinations at 77 K followed by BET theory work up of the data. Additional information was acquired from water vapor adsorption isotherms due to the high polarity of this adsorbate and resulting specific interactions with adsorbent surfaces. Water is a relatively small molecule and, therefore, can penetrate very small pores which are not accessible for nitrogen at the cryogenic temperature of the BET determination. Unique selectivities of adsorption for the hydrogen and carbon dioxide gases were also measured for these GaN nanopowders.

2. EXPERIMENTAL

2.1. Preparation of Samples

The anaerobic synthesis method, developed by some of the co-authors, was applied to make a broad range of GaN nanopowders [17-20]. This method utilizes an oxygen-free gallium compound, gallium dimetylamide $Ga[N(CH_3)_2]_3$. First, the compound undergoes transamination/deamination reactions in refluxing liquid am-

*Address correspondence to this author at the AGH University of Science and Technology, Faculty of Energy and Fuels, al. Mickiewicza 30, 30-059 Krakow, Poland; Tel: +48 12 6174636; E-mail: czepir@agh.edu.pl

1875-6786/13 $58.00+.00

monia to form a solid polymeric gallium imide $[Ga(NH)_{3/2}]_n$. This precursor is subsequently pyrolyzed at various temperatures, *i.e.*, 623 K (sample 1), 723 K (sample 2), 873 K (sample 5), and 1073 K (sample 6) for 4 h under an ammonia flow of 0.2 dm^3/min to yield nanocrystalline GaN powders with a range of crystallite sizes in the low nanosized region. Additionally, two samples are prepared by pyrolysis of the imide at 723 K (i) under dynamic vacuum (sample 3) and (ii) under a N_2 flow of 0.2 dm^3/min (sample 4).

2.2. Characterization

All products were characterized by standard powder XRD diffraction (Siemens D5000 or X'Pert Pro Panalytical with Cu K_α source; 2Θ, 20-80°). Average crystallite sizes were evaluated from the XRD data (see, Supporting Material) with the common Scherrer equation applying the Rietveld refinement method [21] and including a critical appraisal of such results for nanocrystalline GaN as previously discussed by the co-authors [12d] . For the evaluation, changes of the line profile parameters compared to a standard sample were utilized. Our standard was a polycrystalline alumina sintered body with an average grain size over 5 μm subjected to stress relief annealing. Helium densities were determined with Micromeritics AccuPyc. The pore structure of the samples was characterized with a standard physical adsorption of nitrogen at 77 K in a Micromeritics Gemini V-2380 automatic adsorption apparatus. Prior to all adsorption measurements, the samples were degassed at 573 K for one hour under dynamic vacuum. Carbon dioxide, hydrogen, and water vapor physisorption measurements were carried out at 273 K, 77 K, and 295 K, respectively, using the gas adsorption analyser Quantachrome Autosorb-1C.

3. RESULTS AND DISCUSSION

3.1. Characteristics of GaN Nanopowders

The GaN nanopowders were produced by the original anaerobic method *via* the preparation of the gallium imide precursor and its subsequent pyrolysis at various temperatures in the range 623-1073 K [12d, 16-20]. This method provides a convenient route to GaN nanopowders with only residual oxygen contents and controlled average crystallite sizes. The latter can be achieved by utilization of a suitable pyrolysis temperature and a type of gas atmosphere (ammonia, nitrogen or vacuum). The pyrolysis under ammonia at temperatures up to 1073 K was applied to limit the average crystallite sizes in the low 1-17 nm range. Additionally, the application of nitrogen atmosphere or vacuum at 723 K was intended to look into changes of pore structure that are dependent on this factor. At this time, it is worth to point out that higher temperatures than 1073 K afford larger crystallites of up to several tens of nanometers and, consequently, such powders become much less porous with specific surface areas of a few m^2/g [16] and, therefore, negligible adsorption properties.

The average crystallite sizes for the powders included in Table **1** were calculated from the XRD patterns with Scherrer equation applying the Rietveld refinement method [21]. For the evaluation, changes of the line profile parameters compared to a standard sample were utilized. Our standard was a polycrystalline alumina sintered body with an average grain size over 5 μm subjected to stress relief annealing. The profile parameters depend on the instrument settings used for data collection and on the profile function used for the refinement. In our analysis, the full Voigt function was used to describe the profile of the measured diffraction lines. The total profile width is a convolution of the Gaussian profile part and of the Lorentzian profile part and these parts are combined numerically. In such a method, the full width at half maximum (fwhm) is only one of a few fitted parameters. The extremely broad diffraction peaks for the GaN samples could successfully be fitted with the major cubic polytype and residual hexagonal polytype. As extensively discussed in our previous reports [12d, 16], the average crystallite sizes are merely decent approximations for the major polytype due to the extreme peak broadness and overlapping but also because the nanocrystals of GaN in the low nanosized range show a defected structure. Such a structure may be formally described either as cubic or defected heaxagonal. In our opinion, the consistent procedure for sample preparation, pattern recording, and data analysis makes the calculated sizes appropriate for comparison purposes.

The varying helium densities and their values much below the theoretical density for bulk GaN, *i.e.*, 6.1 g/cm^3, indicate a significant agglomeration of the nitride crystallites with some interior spaces impenetrable by helium atoms (Table **1**). This, definitely, has practical consequences for the interpretation of the adsorption data [16].

3.2. Characterization by Nitrogen Adsorption

The nitrogen adsorption/desorption isotherms were typical for adsorbents with the mesoporous structure. According to the IUPAC classification, the shape of the isotherms is of type IV with a hysteresis loop of type H1-H2, the latter characteristic of cylindrical pores. The nitrogen adsorption data were worked up using the standard theoretical approaches. The parameters of interest included the BET (Brunauer-Emmett-Teller) specific surface area, pore volume, and BJH (Barrer-Joyner-Halenda) pore size distribution as described in much of the general literature on this topic. The average pore diameter was calculated from the BET surface area and pore volume. The results of the nitrogen physisorption measurements calculated according to International Standards [22] as well as the data on average crystallite sizes and helium densities are listed in Table **1**.

The sample numbering from 1 to 6, in general, reflects higher and higher pyrolysis temperatures of the gallium imide precursor and coincides with the decreasing BET values for the GaN nanopowders, the latter spanning the range from the highest 287 m^2/g (sample 1) down to the lowest 23 m^2/g (sample 6). These BET values cover the highest specific surface areas reported to-date for mostly mesoporous GaN [14-16] while excluding powders with areas in a few to several m^2/g range that are prevailingly macroporous and, therefore, not expected to exhibit any appreciable adsorption behavior. It is interesting to note that three samples obtained at 723 K under otherwise variable pyrolysis conditions, *i.e.*, samples 2, 3, and 4, differ with many properties. For instance, changing of the kind of gas atmosphere utilized in the preparation of powders, *i.e.*, ammonia (sample 2) *vs.* nitrogen (sample 4), or using instead dynamic vacuum (sample 3) results in various BET surface areas and average pore widths. Sample 3 shows among these materials the remarkably low BJH surface area and the associated pore volume in the mesopore range 1.7-300 nm which together with its lowest BET-derived average pore width supports a significant share of microporosity. In general, the higher is the pyrolysis temperature of the imide precursor the lower is the BET surface area of the resulting GaN nanopowder. This is paralleled more or less closely by an increase in the same fashion of the XRD-derived average crystallite sizes and helium densities of the GaN powders. Interestingly, for both the XRD and helium density data a local minimum is observed in the smallest size range (see Table **1**, samples 3 and 4).

3.3. Water Vapor Adsorption Characteristics

The adsorption/desorption isotherms of water vapor H_2O determined at 295 K are shown for all samples in Fig. (**1**). According to the IUPAC classification, isotherms of this kind belong to type II and describe a multilayer water vapor adsorption in a wide range of relative pressures. At low relative pressures water molecules penetrate the accessible nitride surface first forming a monomolecular layer while at higher pressures a multilayer formation takes place onto the initially adsorbed monolayer. The isotherm is the result of unrestricted monolayer/multilayer adsorption on the heterogeneous substrate and its characteristic features are influenced by the rela-

Table 1. Results of Nitrogen Physisorption, Crystallite Size, and Density Measurements

Sample No.	1	2	3	4	5	6
Pyrolysis temperature and gas atmosphere, K/gas	623/NH_3	723/NH_3	723/vac	723/N_2	873/NH_3	1073/NH_3
BET specific surface area, m^2/g	287	246	179	165	72	23
Total pore volume of pores less than 200 nm (at $p/p_s = 0.99$), cm^3/g	0.218	0.212	0.099	0.096	0.228	0.215
Average pore width, nm	2.76	3.42	1.76	2.27	12.5	35.8
Total pore volume of pore less than 2.7 nm (at $p/p_s = 0.30$), cm^3/g	0.142	0.120	0.092	0.081	0.036	0.012
BJH cumulative volume of pores between 1.7 and 300 nm width, cm^3/g	0.219	0.159	0.018	0.089	0.172	0.038
BJH cumulative surface area of pores between 1.7 and 300 nm width, m^2/g	358	246	30	153	103	41
BJH average pore width, nm	2.42	2.62	2.37	2.43	7.57	6.38
XRD average crystallite size, nm	1.6	1.8	1.2	1.0	3.0	17.0
Helium density, g/cm^3	4.0	4.5	3.8	3.6	5.2	5.0

tive magnitude of both the adsorbent-adsorbate and adsorbate-adsorbate interactions.

The analysis of the adsorption/desorption data reveals the nature of the nitride surfaces and their polarity. The shift of the adsorption branch to high relative pressure indicates both mesoporosity and, generally, rather weak interactions between the inner surface and the polar water molecules as an adsorptive. The desorption branch of the isotherms shows a large hysteresis due to forming the hydrogen bonds among water molecules and it can be explained as resulting from significant energy barriers necessary to overcome these relatively strong interactions. This phenomenon is likely to be accompanied by chemisorption of water molecules on the primary adsorption centers as explained below.

For detailed data analysis, we applied the Generalized D'Arcy and Watt (GDW) model that was developed for description of water adsorption on activated carbons and, subsequently, successfully applied to water adsorption on various foodstuff [23]. It can be formulated as shown below in Equation 1

$$a = \frac{m \cdot K_p \cdot (p/p_s)}{1 + K_p \cdot (p/p_s)} \cdot \frac{1 - K_s \cdot (1-w) \cdot (p/p_s)}{1 - K_s \cdot (p/p_s)} \quad (1)$$

where: m is the maximum sorption capacity on the primary adsorption centers, K_p and K_s are the kinetic constants related to adsorption on the primary and secondary centers, and w is the parameter determining the ratio of molecules bonded to primary center and converted into the secondary ones. The values of the parameters were obtained by nonlinear regression analysis with minimization of the relative deviations between the experimental and predicted values. The calculated maximum relative deviations did not exceed ±3 %.

The parameters of the GDW model are related to the number of primary (m_p) and secondary (m_s) centers *via* the relationships shown in Equations 2 and 3, respectively [24].

$$m_p = \frac{m \cdot K_p + K_s \cdot (1-w)}{K_p + K_s} \quad (2)$$

$$m_s = \frac{m \cdot K_p \cdot w}{K_p + K_s} \quad (3)$$

The values of the GDW parameters as well as the calculated numbers of the primary and secondary centers are listed in Table **2**.

Table 2. Parameters of the Generalized D'Arcy and Watt Model

Sample No.	1	2	3	4	5	6
m, mmol/g	1.053	0.853	0.379	3.162	0.757	0.161
K_p	16.645	30.250	44.649	9.503	61.496	23.475
K_s	0.794	1.021	1.098	1.047	0.949	1.081
w	0.036	0.912	0.862	0.193	1.099	1.062
m_p, mmol/g	1.051	0.827	0.371	3.101	0.745	0.153
m_s, mmol/g	0.036	0.753	0.319	0.551	0.820	0.163

From the critical overview of the kinetic constants it can be concluded that water is likely adsorbed on GaN in two forms, *i.e.*, primary molecules on adsorption sites with high binding energy such as (i) spurious hydroxyl groups, residual amine groups, surface metal atoms and (ii) secondary molecules on sites with relatively lower binding energies such as the previously occupied primary centers and other kinds of secondary sites with low interaction energies.

It is instructive to point out that two of the samples, *i.e.*, sample 1 and sample 4, show the relatively increased numbers of the primary adsorption centers that are accompanied by the lowest values of their respective kinetic constants K_p. The remaining samples are characteristic of the approximately comparable m_p/m_s ratios close to 1. Also, a *ca.* 6-fold spread in the K_p values among the samples points out to a broad differentiation of their surface characteristics. Interestingly, sample 4 with the outstanding high number of primary centers shows also the lowest helium density and the smallest average crystallite size among the samples (Table **1**). The low helium density is indicative of a pronounced crystallite agglomeration while the small crystallite dimension favors extensive surface derivatization consistent with an increased number of primary adsorp-

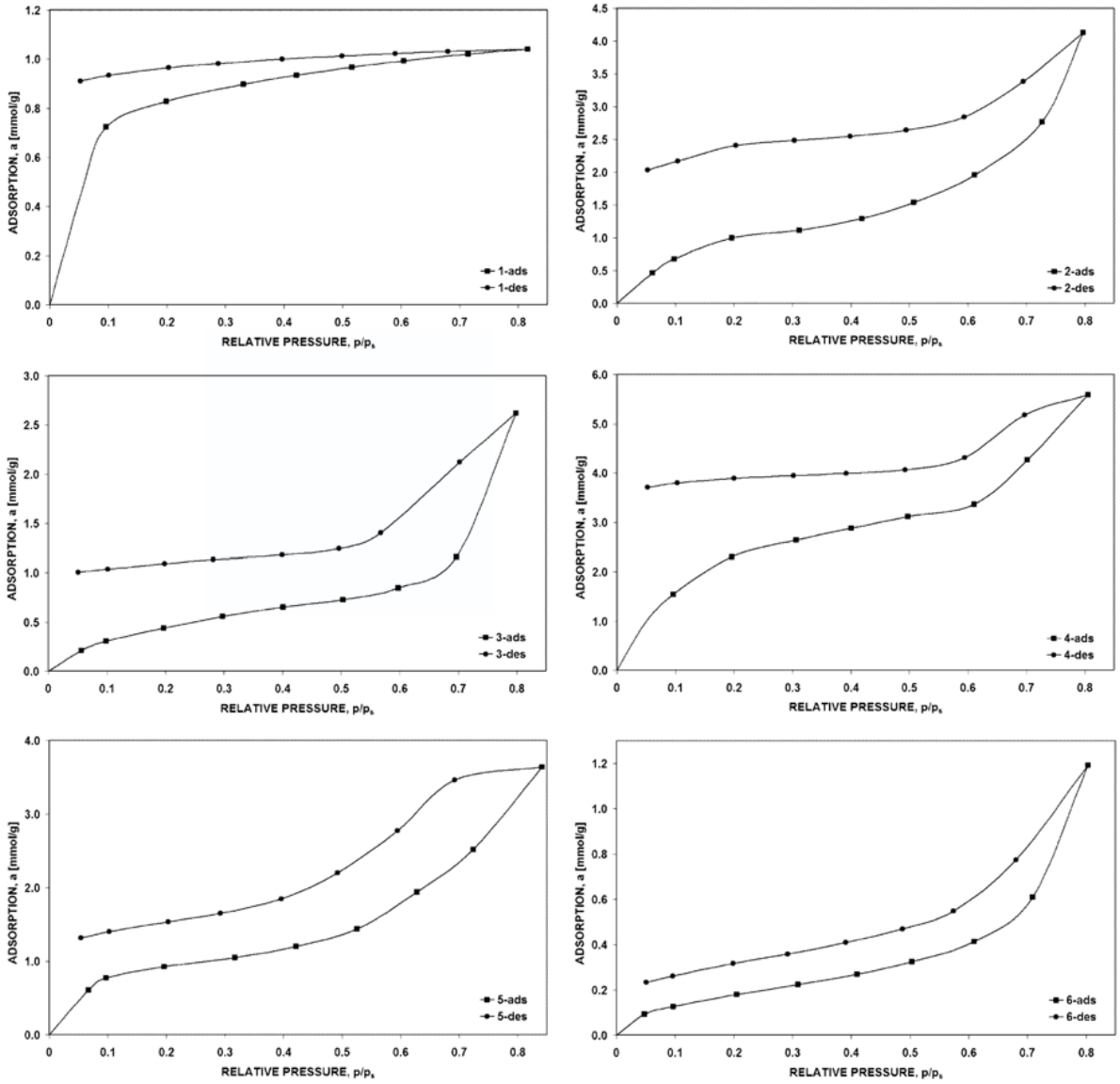

Fig. (1). Water vapor adsorption/desorption isotherms for nanocrystalline powders of gallium nitride.

tion centers – the sources of likely chemical and/or very strong hydrogen bonding interactions with water molecules.

3.4. Adsorption of Hydrogen and Carbon Dioxide

Adsorption of hydrogen H_2 and carbon dioxide CO_2 was investigated at the temperatures of 77 K and 273 K, respectively, in the pressure range 0-760 Torr. The isotherms for all samples are presented in Figs. (**2**, **3**). For both gases the adsorption isotherms are fully reversible which means that H_2 and CO_2 are exclusively adsorbed *via* physisorption.

The maximum adsorption values for hydrogen at 760 Torr are somewhat positively correlated with the sample BET surface areas. This suggests that the physical adsorption prevails being based on local interactions between the hydrogen molecules and particle surface active sites (Table **1**). In this regard, the physisorption is, in general, determined by short-range ordering, curvature, functional groups, and possible defects on the surface. However, there are notable exceptions to this trend exemplified by sample 1 with the highest BET surface area that, at the same time, shows the lowest hydrogen adsorption. Also, sample 3 displays the markedly highest hydrogen adsorption capacity while showing still a smaller BET surface area than samples 1 and 2. The specific feature of sample 3 is the highest share od microporosity among the samples that is accompanied by a significant crystallite agglomeration (low helium density). All this means that the interplay of pore size distribution and extent of agglomeration are the additional important factors effecting the hydrogen physisorption in the system. Finally, the pool of the GaN nanopowders yields the hydrogen adsorption capacities differing by one order of magnitude (Fig. **2**). In our opinion, the results constitute a solid starting point to consider these materials for hydrogen gas sensors.

For carbon dioxide CO_2, somewhat different trends are observed than discussed above for hydrogen which means that the adsorption mechanism for CO_2 is quite different and connected mainly with volume filling of mesopores. In sharp contrast to the hydrogen adsorption data, sample 1 presents now the highest and sample 3 the lowest adsorption capacities – a remarkably reversed order (Fig. **3**). Actually, the order of descending carbon dioxide adsorption capacities follows nicely the descending order of the BJH cumulative volume of pores with width between 1.7 and 300

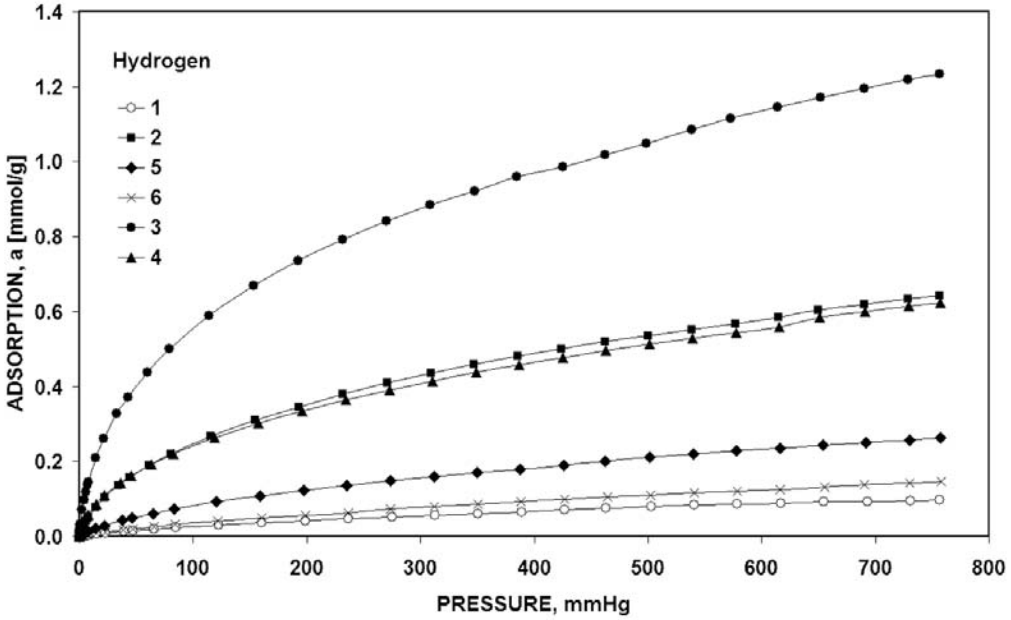

Fig. (2). Hydrogen adsorption isotherms for nanocrystalline powders of gallium nitride.

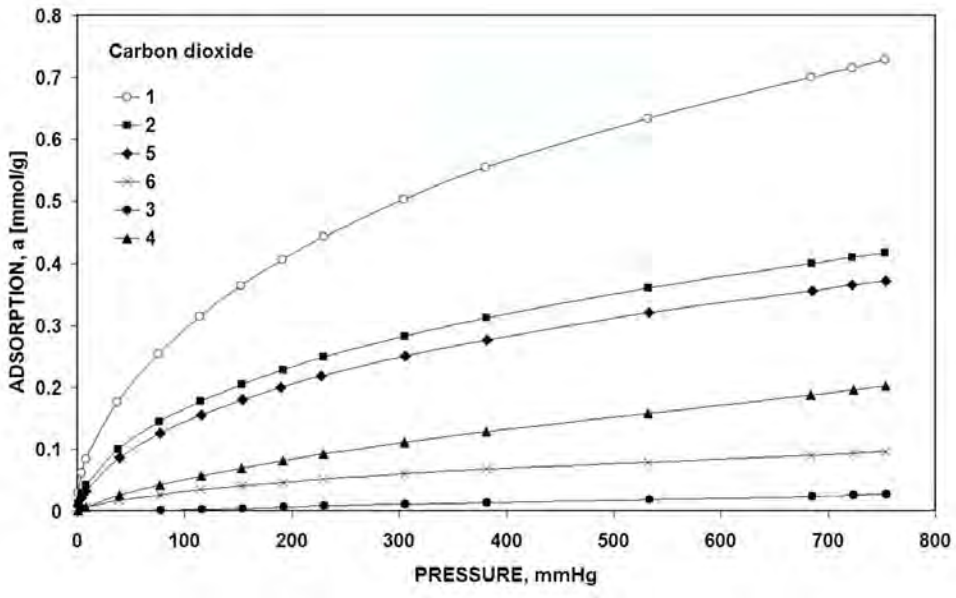

Fig. (3). Carbon dioxide adsorption isotherms for nanocrystalline powders of gallium nitride.

nm (Table **1**) supporting the volume condensation mechanism in the mesopores. In this regard, we want to point out that the established spread in adsorption capacities of one order of magnitude is paralleled by a *ca.* tenfold change in the BJH cumulative mesopore volumes.

We furthermore attempted to estimate the selectivity of the samples towards adsorption of carbon dioxide and hydrogen. It was found that the Langmuir isotherm gives a satisfactory representation of the adsorption data. Herein, selectivity is defined as the ratio of the respective Henrys' constants, K_H, calculated from the Langmuir equation (Table **3**). As a common trait in the entire study, also in this case a diverse selectivity characteristics is observed encompassing, on the one end, sample 1 with a prevailing affinity for carbon dioxide and, on the other end, sample 3 with a strong preference for hydrogen and negligible adsorption of carbon dioxide. In between of the two extremes, sample 6 shows no apparent selectivity towards these gases. The results support a notion that some of the GaN nanopowders could be considered promising candidates for efficient separation of such gas mixtures.

4. CONCLUSIONS

Systematic variations of synthesis conditions result in the nanocrystalline GaN powders with pore structure and adsorption properties each varying over a fairly wide range. The main experimental factors influencing the adsorption properties of the nanopowders are the pyrolysis temperature and the kind of gas atmosphere (or its lack if vaccum is applied) during the thermally driven decomposition of the gallium imide precursor.

The study shows that the pore structure of such nanopowders is prevailingly mesoporous and it can be tailored toward products with

Table 3. Adsorption Selectivities with Respect to Carbon Dioxide and Hydrogen

$K_H \cdot 10^4$ [mmol/g·Torr]	Sample No.					
	1	**2**	**3**	**4**	**5**	**6**
Carbon dioxide, CO_2	40.3	22.2	0.4	5.3	18.8	3.6
Hydrogen, H_2	2.7	34.0	94.4	33.4	9.1	3.5
Selectivity, $K_H(CO_2)/K_H(H_2)$	15.0	0.65	0.004	0.16	2.07	1.03

desired adsorption properties and gas selectivities. The pronounced selectivies towards physisorption of hydrogen and carbon dioxide are the unique assets of the materials. On the other hand, water vapor appears to be adsorbed strongly *via* chemisorption and this may have a crucial impact on many applications of the nanopowders. With the general trends established, a number of processing parameters needs to be fine-tuned to optimize the pore structure characteristics suitable for a selected application. Also, investigations of gas-specific adsorption from appropriate gas mixtures will be necessary to address the realistic adsorption selectivities towards various gases in the mixtures. Some of these issues are currently followed up in our laboratories.

CONFLICT OF INTEREST

The authors confirm that this article content has no conflicts of interest.

ACKNOWLEDGEMENTS

The study was supported by the Ministry of Science and Higher Education/MNiSW (Poland), Grant No. N N507 4435 34.

REFERENCES

[1] Arakawa, Y. Progress in GaN-based quantum dots for optoelectronic applications. *IEEE J. Sel. Top. Quant. Elect.,* **2002**, *8*, 823-832.

[2] Akasaki, I.; Amano, H. Crystal Growth and Conductivity Control of Group III Nitride Semiconductors and Their Application to Short Wavelength Light Emitters. *Jpn. J. Appl. Phys.,* **1997**, *36*, 5393-5408.

[3] Han, W.; Zettl, A. Pyrolysis approach to the synthesis of gallium nitride nanorods. *Appl. Phys. Lett.*, **2002**, *80*, 303-305.

[4] Nakamura, S. InGaN-based blue light-emitting diodes and laser diodes. S. *J. Cryst. Growth,* **1999**, 201-202, 290-295.

[5] Strite, S.; Morkoç, H. GaN, AlN, and InN: A review. *J. Vac. Sci. Technol. B,* **1992**, *10*, 1237-1266.

[6] Janik, J. F.; Drygas, M.; Czosnek, C.; Kamińska, M.; Palczewska, M.; Paine, R. T. Carbothermally-assisted aerosol synthesis of semiconducting materials in the system GaN/Mn. *J. Phys. Chem. Sol.*, **2004**, *65*, 639-645.

[7] Uthirakumar, P.; Ryu, B. D.; Kang, J. H.; Kim, H. G.; Hong, C. H. Impact of Nano-Texturing in GaN-based Light Emitting Diodes by Self-Assembled Silver Microspheres as Etch Mask. *Curr. Nanosci.*, **2011**, *7*(6), 1000-1003.

[8] Li, X.; Kim, Y.-W.; Bohn, P. W.; Adesida, I. In-plane bandgap control in porous GaN through electroless wet chemical etching. *Appl. Phys. Lett.*, **2002**, *20*, 980-982.

[9] Steven-Kalceff, M. A.; Tiginyanu, I. M.; Langa, S.; Foll, H.; Hartnagel, H. L. Correlation between morphology and cathodoluminescence in porous GaP. *J. Appl. Phys.*, **2001**, *89*, 2560-2565.

[10] Mynbaeva, M.; Bazhenov, N.; Mynbaev, K.; Evstropov, E.; Saddow, S. E.; Koshka Y.; Melnik, Y. Photoconductivity in Porous GaN Layers. *Phys. Status Solidi B*, 2001, *228*, 589-592.

[11] Xu, Q. J.; Zhang, S. Y.; Zhuang, H. Z. Synthesis of Probe-Shaped GaN Nanorods by Ammoniating Ga_2O_3/Mo Films. *Curr. Nanosci.*, **2009**, *5*(3), 289.

[12] (a) Stelmakh, S.; Swiderska-Sroda, A.; Kalisz, G.; Gierlotka, S.; Grzanka, E.; Palosz, B.; Drygas, M.; Janik, J. F.; Paine, R. T. Microstructure and mechanical properties of GaN nanoceramics sintered under high-pressure-high-temperature conditions. *Proceedings of the International Conference on Nanoscience and Technology*, Basel, Switzerland, July 30-August 4, 2006; Institute of Physics Publishing: Philadelphia, PA, **2006**; p. 1399.

(b) Grzanka, E.; Stelmakh, S.; Gierlotka, S.; Swiderska-Sroda, A.; Kalisz, G.; Palosz, B.; Drygas, M.; Janik, J. F.; Paine, R. T. In situ X-ray diffraction studies of distribution of strain during simultaneous sintering of nanocrystalline GaN powders under high-pressure high-temperature conditions. *European Powder Diffraction Conference, EPDIC-10*, Geneva, Switzerland, Sept 1-4, **2006**; also, in *Z. Kristallogr.*, **2007**, *26*, MS11-P92.

(c) Borysiuk, J.; Caban, P.; Strupinski, W.; Gierlotka, S.; Stelmakh, S.; Janik, J. F. TEM investigations of GaN layers grown on silicon and sintered GaN nano-ceramic substrates. *Cryst. Res. Technol.*, **2007**, *42*, 1291.

(d) Drygas, M.; Olejniczak, Z.; Grzanka, E.; Bucko, M. M.; Paine, R. T.; Janik, J. F. Probing the structural/electronic diversity and thermal stability of various nanocrystalline powders of gallium nitride GaN. *Chem. Mater.*, **2008**, *20*, 6816-6828.

(e) Drygas, M.; Bucko, M. M.; Olejniczak, Z.; Grzegory, I.; Janik, J. F. High temperature chemical and physical changes of the HVPE-prepared GaN semiconductor. *Mater. Chem. Phys.*, **2010**, *122*, 537-543.

(f) Janik, J. F.; Drygaś, M.; Czosnek, C.; Pałosz, B.; Gierlotka, S.; Stelmakh, S.; Grzanka, E.; Kalisz, G.; Świderska-Środa, A.; Leszczyński, M.; Nowak, G.; Czernecki, R. *Polish Patent No. 378458*, published in WUP 02/12, Feb. 29, 2012 (in Polish).

[13] Yam, F. K.; Hassan, Z.; Chuah, L. S.; Ali, Y. P. Investigation of structural and optical properties of nanoporous GaN film. *Appl. Surf. Sci.*, **2007**, *253*, 7429-7434.

[14] Czepirski, L.; Janik, J. F.; Komorowska-Czepirska, E.; Wells, R. L. Adsorption characteristics of powders of nanometric gallium nitride and aluminum nitride. *Adsorpt. Sci. Technol.*, **2002**, *20(8)*, 723-728.

[15] (a) Chaplais, G.; Schlichte, K.; Stark, O.; Fischer, R. A.; Kaskel, S. Template Assisted Design of Microporous Gallium Nitride Materials. *Chem. Commun.*, **2003**, 730-731. (b) Chaplais, G.; Kaskel, S. Porosity Control in Pre-Ceramic Molecular Precursor-Derived GaN Based Materials. *J. Mater. Chem.*, **2004**, *14*, 1017-1025.

[16] Drygas, M.; Janik, J. F. Modeling porosity of high surface area nanopowders of the gallium nitride GaN semiconductor. *Mater. Chem. Phys.*, **2012**, *133*, 932-940.

[17] Janik, J. F.; Wells, R. L. Gallium Imide, $\{Ga(NH)_{3/2}\}_n$, a New Polymeric Precursor for Gallium Nitride Powders. *Chem. Mater.*, **1996**, *8*, 2708-2711.

[18] Wells, R. L.; Janik, J. F.; Gladfelter, W. L.; Coffer, J. L.; Johnson, M. A.; Steffey, B. D. New Precursor Routes to Nanocrystalline Cubic/Hexagonal Gallium Nitride GaN. *Mater. Res. Soc. Symp. Proc.*, **1997**, *3*, 468.

[19] Coffer, J. L.; Johnson, M. A.; Zhang, L.; Wells, R. L.; Janik, J. F. Influence of Precursor Route on the Photoluminescence of Bulk Nanocrystalline Gallium Nitride. *Chem. Mater.*, **1997**, *9*, 2671-2673.

[20] Wells, R. L.; Gladfelter, W. L. Pathways to Nanocrystalline III-V (13-15) Compound Semiconductors. *J. Cluster Sci.*, **1997**, *8*, 217-238.

[21] Klug, P. H.; Alexander, E. L. *X-ray Diffraction Procedures*, John Wiley & Sons, New York, **1974**.

[22] ISO 9277:2010(E), Determination of the specific surface area of solids by gas adsorption – BET method; ISO 15901-2:2006(E), Pore size distribution and porosity of solid materials by mercury porosimetry and gas adsorption – Part 2: Analysis of mesopores and macropores by gas adsorption; ISO 15901-3:2006(E), Pore size distribution and porosity of solid materials by mercury porosimetry and gas adsorption – Part 3: Analysis of micropores by gas adsorption.

[23] Furmaniak, S.; Terzyk, A. P.; Golembiewski, R.; Gauden, P. A.; Czepirski, L. Searching the Most Optimal Model of Water Sorption on Foodstuffs in the Whole Range of Relative Humidity. *Food Res. Int.*, **2009**, *42*(8), 1203-1214.

[24] Furmaniak, S.; Terzyk, A. P.; Gauden, P. A. Some Remarks on the Classification of Water Vapor Sorption Isotherms and Blahovec and Yanniotis Isotherm Equation. *Dry. Technol.*, **2011**, *29*, 984-991.

Received: September 25, 2012 Revised: November 2, 2012 Accepted: December 13, 2012